IBM Research Report

Practical Considerations in the Modeling and Characterization of Printed-Circuit Board Wiring

A. Deutsch, R. Krabbenhoft[1], C. W. Surovic, T-M. Winkel[2], C. Schuster, Y. Kwark, E. Klink[2]

IBM Research Division
Thomas J. Watson Research Center
P.O. Box 218
Yorktown Heights, NY 10598

[1]IBM Systems and Technology Group
Rochester, MN

[2]IBM Systems and Technology Group
Boeblingen, Germany

IBM

Research Division
Almaden - Austin - Beijing - Haifa - India - T. J. Watson - Tokyo - Zurich

Practical Considerations in the Modeling and Characterization of Printed-Circuit Board Wiring

A. Deutsch, R. Krabbenhoft[1], C. W. Surovic, T-M. Winkel[2], C. Schuster, Y. Kwark, , E. Klink[2]

IBM T. J. Watson Research Center, 1101 Kitchawan Road, Yorktown Heights, N.Y. 10598,

Phone: (914) 945-2858, Fax: (914) 945-2141, email:deutsch@us.ibm.com

[1]IBM Systems and Technology Group, Rochester, MN

[2]IBM Systems and Technology Group, Boeblingen, Germany

Abstract

The importance of increased accuracy in modeling and characterization of printed-circuit board wiring is highlighted through practical examples. Recommendations are given regarding model causality, bandwidth, measurement methodology improvement for both production-level and off-line monitoring of impedance, roughness, and dielectric loss and their significance for system design, performance, delivery, and cost is discussed.

Introduction

The continued increase in data-rates transmitted on long printed-circuit board interconnects require increased modeling and characterization accuracy and bandwidth. Typical data transmission in digital applications involves a variable data pattern with very fast transitions and long spans of steady-state levels. This implies that both the models representing these lossy transmission lines and the measurements need to be broadband in nature, from DC to close to 50 GHz for systems delivered in the 2005-2010 timeframe [1]. Many of the effects that could be ignored in the past at lower frequencies are gaining significance. Each component in a critical path contributes to signal distortion and affects system performance. Due to the need for lower power densities while also operating at higher frequencies, smaller swing signals are being used. Noise sources and reflections are becoming larger detractors from signal integrity and consuming the entire noise budget. This is why the properties of each component in the critical path have to be modeled and characterized with greater accuracy and at higher frequencies.

Broadband complex permittivity extraction of card insulators obtained on representative multi-layer structures is required. Accurate accounting of the roughness of the metallization and its impact on the total interconnect loss has to be made. Causal transmission line models have to be generated for accurate system performance prediction. Newer insulator materials with lower loss, lead-free compatibility, and better thermal and mechanical properties are being developed. Evaluation of the merits of such materials needs to be made with much greater accuracy even in the manufacturing environment. This leads to a closer scrutiny and redesign of the production-level process monitoring coupons currently used. Measurement of impedance needs to be extended to include frequency-dependent interconnect losses and dielectric material properties.

In this paper, examples are given of some of the changing requirements for both modeling and measurement of representative printed-circuit interconnect characteristics and their relevance for overall system performance, delivery, and cost is explained.

Complex Permittivity Extraction

a. Causal Predictive Models

The increase in system integration density with time results in the use of narrower line widths of 3 – 5 mil and 0.5 to 1 oz copper thickness (0.6 – 1.2 mil). Losses caused by both skin-effect and dielectric dispersion affect the risetime dispersion and signal delay. These losses need to be accurately included in system prediction simulations. Fig. 1 shows examples of representative stripline structures that were modeled with only skin-effect (tanδ = 0), with skin-effect and roughness (tanδ = 0), and with skin-effect, rough ridges, and complex frequency-dependent permittivity. The increase in attenuation due to dielectric loss starts to substantially dominate resistive losses for the lower resistance, 5-mil wide lines, even at as low a frequency as 5 GHz. Roughness also contributes a substantial amount to total loss.
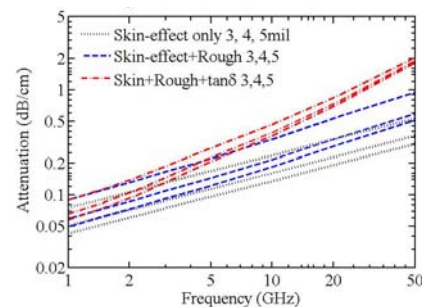

Fig. 1 Calculated attenuation insulator for 3.0 mil 0.5 oz, 4 mil 1 oz, and 5 mil, 1 oz lines with card B material.

Designers need accurate material parameters from suppliers in order to generate predictive models. Suppliers will provide the DC copper resistivity but not the surface treatment used for the roughening process. Dielectric constant and dielectric loss are generally supplied at a few frequencies, several, non-consistent techniques, over different frequency ranges are combined, and most often, using bulk materials rather than representative, multilayer laminates. Such techniques might also miss inhomogeneities in the effective dielectric properties that are of interest for signal propagation on typical card wiring.

Characteristic impedance is measured in TDR but the broadband $Zo(f)$ is not available. Attenuation might be measured at a few frequencies for a specific cross section, often times not on multi-layer structures. Measurements made in the frequency-domain are complex, costly, not consistent across suppliers, and were shown [2] not to be able to extract the broadband permittivity.

It has been proposed to use a Debye model to represent the slowly varying $\varepsilon_r^{'}(f)$ and tan$\delta(f)$ properties of most printed-

circuit board insulator materials. It ensures causality for $\varepsilon(f)$ and is a good representation for the polarization-damping based losses. The analytic function below

$$\varepsilon(\omega) = \varepsilon_\infty + \sum_i \frac{\varepsilon_i}{1 + j\omega\tau_i} \qquad (1)$$

can be calculated with a small number of poles. A typical representation for a good broadband model might have 30 poles over the range 10 KHz to 1000 GHz. Ten values could be specified and interpolation and piecewise linear expansion with respect to $log(f)$ can be made to consistently determine both $\varepsilon_r^{'}(f)$ and $\tan\delta(f)$ over the desired frequency range.
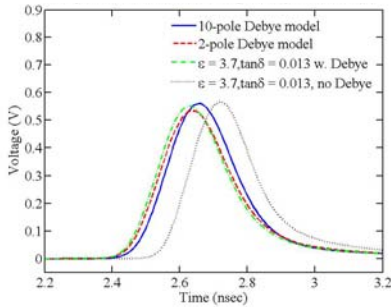

Fig. 2. Simulated 6 Gbps response for 38 cm trace on card B.

Fig. 2 shows simulation results for a 38 cm long line and 6 Gbps transmission for four conditions. Simulation was made with ten initial $\tan\delta$ values in the range of 10 GHz to 50 GHz, two values, namely at 1 MHz and 50 GHz, constant $\varepsilon_r^{'}$ and $\tan\delta$, and constant values without using a Debye model. It was found that the differences in amplitude were -28.3 mV, -8.5 mV, +6.9 mV compared to the ten-value case with amplitude of 561 mV, respectively. The delay differences were -16 ps, -25 ps, and +70 ps , respectively. The accuracy of the model increases with the number of specified input values, however, all Debye-based models are much closer to each other and to measurements than when causality is not respected. For constant $\varepsilon_r^{'}$ and $\tan\delta$, $G = \omega C\tan\delta$ expression is used with C at 1 MHz and this cannot provide consistency of complex $\varepsilon(f)$ and results in large simulation errors. Measured $\varepsilon_r^{'}(f)$ and $\tan\delta(f)$ are shown in Figs. 3a and b for three card materials based on measurements on representative stripline structures.
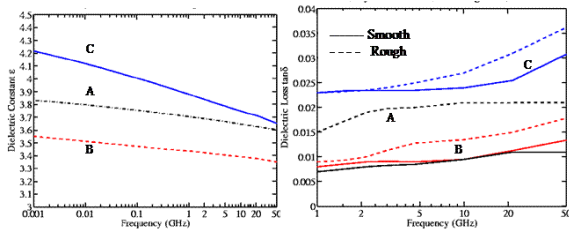

Fig. 3 Extracted $\varepsilon_r^{'}(f)$ for smooth foil and $\tan\delta(f)$ for the six cases of Fig. 4 for cards C (solid), B (dot-dashed), and A (dotted)

b. Short-Pulse Propagation Technique

It has been shown that a very simple time-domain technique can successfully be used to extract the broadband permittivity for typical packaging interconnects. The technique is typically used on representative stripline structures built with small interface discontinuities such as

pads and vias. A short pulse is injected into two lines of different lengths. Signal processing of the digitized pulses consists of rectangular time windowing of the unwanted reflections from interface discontinuities and Fourier transformation. From the ratio of the two Fourier transforms the total attenuation $\alpha(f)$ and phase constant $\beta(f)$ are obtained. $R(f)$, $L(f)$, $C(f)$, and $G(f)$ are calculated using a causally-enforced field solver, CZ2D [3], and the Debye model from (1). The total attenuation $\alpha(f)$ and $\beta(f)$ are fitted to the measured values and smooth interpolation and extrapolation is made over the desired frequency range. The broadband $Zo(f)$ can also be obtained this way from $Zo(f) = G(f)/ (G(f) + 2\pi f C(f))$. Fig. 4 shows the calculated attenuation for the three cards of Fig. 3 having the same cross section but with the material characteristics extracted from measurements of actual card structures with and without roughened foil [4].
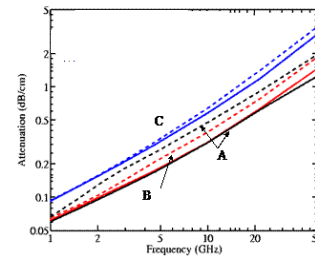

Fig. 4 Calculated attenuations for 4-mil wide lines for Cards A, B, and C with smooth (solid) and rough metallization (dotted).

c Effect of Roughness

It was shown in [5] that resistive losses increase due to roughening of metallization especially at high frequencies. This contribution can be as high as 5.5% to 49.5% even at 5 GHz as can be seen in Fig. 4. The effect of roughness can be quite different in characteristic depending on material used by card supplier and treatment used for the metal foil. The rough ridge profile could even differ on the ground layer from the signal layer within the same stripline cross section. The organo-metallic coating of the lines and the composition of the micro-nodules is not generally released or known by vendors. Because of the unknown resistivity and difficulty in modeling of the complex ridges, when extracting $\varepsilon_r^{'}(f)$ and $\tan\delta(f)$, the effect of roughness which is an additional resistive loss, gets attributed to dielectric loss. Fig. 3b shows the large error in the extracted $\tan\delta(f)$ when the actual topography of the ridges is not accounted for. It was shown in [5] that simplified 2D modeling techniques can be used to generate accurate causal predictive line models but both a rough and a smooth card build are needed for the same cross section. It was also found that roughness used with the newly developed, low-loss, insulators, could cancel the beneficial effects of low $\tan\delta$, especially at high frequencies. The results in Fig. 1 for card B also show the fact that roughness adds a substantial amount of resistive loss while dielectric loss dominance starts at a higher frequency of around 10 GHz for 4 mil, 1 oz lines, for example.

Monitoring of Card Characteristics in Manufacturing
a. Impedance Extraction Loss Compensation

Typical manufacturing process monitoring of printed-circuit boards relies on simple TDR measurement of the characteristic impedance Zo. In-line structures of 6 inch long

lines are measured with fairly standard equipment such as the Polar CITS800S4 [6] and hand held probes. Layouts are shown in Figs. 5a, b, and c with test pads on 100 mil pitch. A side view of such a probe is shown in Fig. 6a.
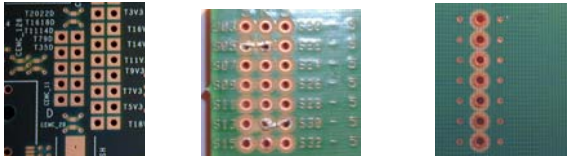

Fig. 5 Coupon layout for a) 90-mil, and b) and c) 140 mil card.
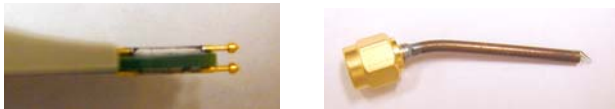

Fig. 6 Side view of a) Polar 100-mil pitch and b) coaxial 10-mil pitch probes.

Because of the long card trace inside the probe, the slow step excitation, and the 100-mil tip pitch, the board trace will typically receive a 200 ps transition.

The long trace on the board "coupon" will exhibit a rising TDR waveform due to all the losses explained earlier as seen in Fig. 7 below.
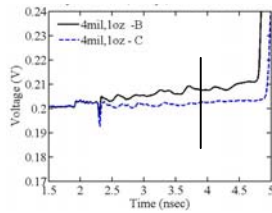

Fig. 7 TDR response on 20 cm trace for cards B (solid) and C (dotted) with 4 mil 1 oz lines.

The characteristic impedance is expressed by

$$Zo = \sqrt{\frac{R + j\omega L}{G + j\omega C}} \qquad (2)$$

and the resistive and dielectric losses will affect the slope of the TDR waveform along the length of the line. Some PCB test equipment suppliers will specify the monitoring of Zo at around a 1.5 ns distance from the start of the actual TDR waveform at T=0 as seen in Fig. 7. This is recommended in order to avoid the uncertainty caused by the reflection at the beginning of the line due to the interface discontinuities and probes. A typical response is shown in Fig. 8 for the coupons of Fig. 5b. For the actual driver circuits charging the long transmission lines, the incident impedance at T=0, $Zo = \sqrt{L/C}$, or impedance without loss affects the driver current and power. Measuring Zo at a distance of 1.5 ns along the line will result in an unrealistically high value due to loss. It should be noted that (2) predicts an exponentially rising behavior. Some simplified linear loss compensation techniques have been suggested.

In order to assess the needed compensation for the actual Zo at T=0, simulations were made with line widths ranging from 3 – 5 mil, 0.5 and 1 oz copper (0.6 and 1.2 mil thick), and single or differential pair configurations and with the material characteristics of the cards B and C in Fig. 3 and roughness included. A very fast (almost ideal step) was used

for exciting a 6-inch long trace. All the cross sections were designed to result in 50 Ω or 100 Ω Zo for single or differential lines, respectively, at infinite frequency.
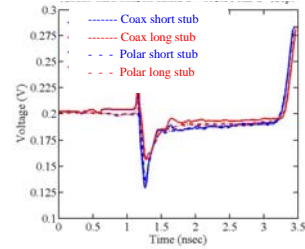

Fig. 8 TDR response for long and short via stub with the two probes of Fig. 6a (dot) and b (solid), on the coupon in Fig. 5b.

The table summarizes the simulated and calculated Zo values.

Table. Simulated Zo at T=0 and Calculated Zo

| Line Config. | Card B | | Card C | |
| | Sim. | √L/C | Sim. | √L/C |
		(Ω)		
Diff5mil,1oz	102.53	99.8	98.22	101.2
Diff4mil,1oz	104.92	101.2	98.89	101.1
Sing5mil,1oz	49.25	50.6	47.32	50.7
Sing4mil,1oz	48.88	50.0	47.09	50.1
Sing3.5mil,1oz	49.80	50.8	47.18	50.1
Sing3mil,1oz	49.69	50.5	47.92	50.6
Sing3mil,0.5oz	49.13	50.2	47.47	50.4

The simulated and calculated result differences depend of the Debye model differences dictated by the values of Fig. 3.
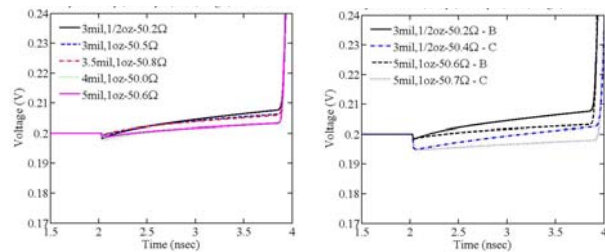

Fig. 9 Single line TDR simulation for a) card B and b) cards B and C. Calculated Zo at infinite frequency are indicated.

Fig. 9a shows a typical set of responses for the card B for the single lines cases with 3mil, 0.5 oz, and 3.0, 3.5, 4.0, and 5.0 mil, 1 oz cross sections. The TDR slope becomes increasingly steeper for the more resistive lines as expected from (2). This is also highlighted in Fig 9b for the 3.0 and 5.0 mil wide lines and cards B and C. Card B has a steeper slope just as seen in the measurement in Fig. 7. Resistive losses will affect this slope the most as seen from Fig. 1 and it was shown in Fig. 3 that the increase in attenuation due to roughness is much stronger for card B than for card C even though card C has higher tanδ. The actual roughness profile was shown in [5] to be much higher for the newer card material B.
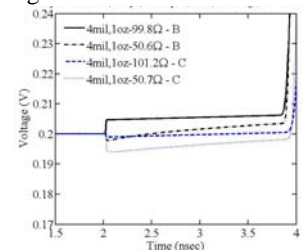

Fig. 10 TDR simulations for single and differential 4-mil cases.

Fig. 10 highlights the difference in behavior between single and differential lines with 4 mil, 1 oz cross section. The differential lines show an extremely shallow slope because the odd-mode of propagation results in a more efficient current return path through the neighboring line than through the ground planes for the single line configuration.

The offset in Zo between the value measured at T = 1.5 ns and T = 0 is plotted in Fig. 11 for the two cards. The higher ε_r and tanδ card C, with much smaller rough ridges, shows a much smaller rate of increase due to resistive losses and the offset is overall smaller. It can be seen from Fig. 11 that the loss compensation offset is very much material and processing dependent and the error in monitored Zo could be in the range of 1.43 – 4.25 Ω for single lines and 1.047 to 1.33 Ω for differential lines for representative cross sections of interest in most common cards. Such offsets have significant system design and cost implications especially for multi-layer large boards that need to accommodate an entire system motherboard and are limited in wiring density and overall thickness. Incorrect Zo results in I/O driver circuit design supplying the incorrect current into the package wiring and thus the system power delivery is impacted.
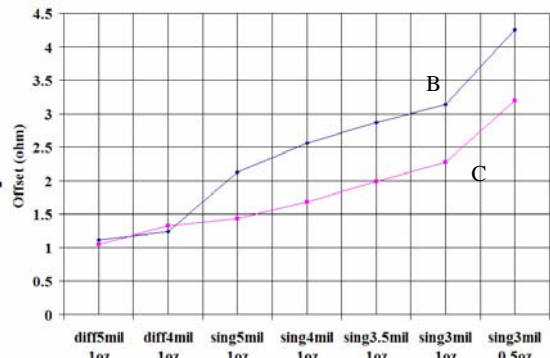

Fig. 11 Zo compensation offset for cards B (circles) and C (squares).

b. Coupon Design

The type of results shown in Fig. 3 with material parameter extraction up to 50 GHz could only be made possible with carefully designed cross sections with minimal interface discontinuities. The higher data rates demand more advanced measurement techniques such as the short-pulse propagation – based methodology. The simple, single-frequency Zo coupon testing will have to be enhanced with attenuation measurement and ultimately the full propagation constant $\Gamma(f)$ and $Zo(f)$ extraction. In Fig. 8 the TDR waveforms obtained with the coarse, 100-mil pitch Polar probe are compared with a 10-mil pitch coaxial probe shown in Fig. 6b. With a 35-ps step excitations, the coaxial probe can transmit a 60 ps risetime while the Polar probe response has only a 120 ps transition. This was measured in reflection on the input TDR trace.

It can be seen in Fig. 8 that due to the faster risetime propagated through the coaxial probes, the inductive discontinuity spikes are visible at the beginning of the line while the Polar probe cannot resolve this effect. Measurements are shown on a top layer with long via stubs and on a lower layer with shorter stub and the reflections reflect this difference. The entire board thickness was 140 mil.

The smaller signal via in Fig. 5c eliminates the capacitive discontinuity but then the inductive discontinuity caused by the large 100-mil separation, not compensated by via capacitance, is clearly visible in a TDR trace. When probing from frontside and backside the pads of Fig. 5a for the thinner, 90 mil thick card, the large square pads introduced larger capacitive discontinuities than the thicker card in Fig. 5b. and they overwhelmed the via stub effect. The short-pulse propagation technique was used for the lines of Fig. 5a for 3 inch and 6 inch lengths and the extracted attenuation bandwidth was only about 3 GHz.

Clearly such coupon designs need to be enhanced for future high-speed data rates. The large discontinuities introduce inaccuracies in the Zo extraction and limit the use of these structures for more advanced techniques. Two different lengths, with small-diameter vias, small signal pads, via constructions with small or no stubs are needed. Any type of advanced analyses require differential measurements between two lengths to eliminate the effect of interface discontinuities.

Conclusions

It has been shown that many of the inaccuracies in modeling and measurement that could be tolerated at 1-3 GHz operation need to be eliminated for the 5-10 GHz regime. These inaccuracies greatly affect the system performance and delivery. Broadband complex permittivity is essential to be determined accurately and used to generate causal predictive models. In spite of the lack of information about the metal roughness properties, a simple technique was shown for quantifying and separating it from dielectric loss. The need for roughness reduction for the newer materials was highlighted. The importance of accurately accounting for all the losses in the process-level coupon monitoring of the characteristic impedance was explained. The loss compensation can have significant impact on the system cost when large multi-layer boards are used. It also affects the total system power due to the impact of the needed I/O circuit current drive specification. Recommendations were made for improving the process coupons to enhance the Zo monitoring and for being able to extend the simple, single-frequency, impedance-only measurement. In the 5-10 GHz operating frequency timeframe, such measurements need to be extended to assessing all frequency-dependent interconnect losses and dielectric material properties.

References

[1] G. Katopis, "Signal Interconnect Trends and Challenges Inside the CEC", http://www.ewh.ieee.org/soc/cpmt/tc12/

[2] T-M. Winkel et al., "Comparison of Time- and Frequency-Domain Measurement Results for Product Related Card and MCM Transmission Lines up to 65 GHz", Digest of EPEP'05, Oct. 24-26, 2005, Austin, TX, pp.21-24.

[3] W. Weeks, "Calculation of Coefficients of Capacitance of Multiconductor Transmisison Lines in the Presence of Dielectric Interface", IEEE Trans. Micr. Th. Tech., MTT-21, pp.76-82, 1973.

[4] A. Deutsch, et al, "Extraction of $\varepsilon_r(f)$ and tanδ(f) for Printed-Circuit Board Insulators up to 30 GHz Using the Short-Pulse Propagation Technique", IEEE Trans. Adv. Packg, vol. 28, no. 1, Feb. 2005.

[5] A. Deutsch, et al, "Losses Caused by Roughness of Metallization in Printed-Circuit Boards", Digest of EPEP'05, Oct. 24-26, 2005, Austin, TX, pp. 39-42.

[6] Polar Instruments, http://www.polarinstruments.com/.